Research Article

The sensor protein AaSho1 regulates infection structures differentiation, osmotic stress tolerance and virulence via MAPK module AaSte11-AaPbs2-AaHog1 in *Alternaria alternata*

Yongxiang Liu [a,b], Jing Yuan [a], Yongcai Li [a,*], Yang Bi [a], Dov B. Prusky [a,c]

[a] *College of Food Science and Engineering, Gansu Agricultural University, Lanzhou, China*
[b] *College of Horticulture, Xinyang Agriculture and Forestry University, Xinyang, China*
[c] *Institute of Postharvest and Food Sciences, Agricultural Research Organization Volcani Center Information Center, Rishon LeZion, Israel*

A B S T R A C T

The high-osmolarity-sensitive protein Sho1 functions as a key membrane receptor in phytopathogenic fungi, which can sense and respond to external stimuli or stresses, and synergistically regulate diverse fungal biological processes through cellular signaling pathways. In this study, we investigated the biological functions of *AaSho1* in *Alternaria alternata*, the causal agent of pear black spot. Targeted gene deletion revealed that AaSho1 is essential for infection structure differentiation, response to external stresses and synthesis of secondary metabolites. Compared to the wild-type (WT), the ΔAaSho1 mutant strain showed no significant difference in colony growth, morphology, conidial production and biomass accumulation. However, the mutant strain exhibited significantly reduced levels of melanin production, cellulase (CL) and ploygalacturonase (PG) activities, virulence, resistance to various exogenous stresses. Moreover, the appressorium and infection hyphae formation rates of the ΔAaSho1 mutant strain were significantly inhibited. RNA-Seq results showed that there were four branches including pheromone, cell wall stress, high osmolarity and starvation in the Mitogen-activated Protein Kinase (MAPK) cascade pathway. Furthermore, yeast two-hybrid experiments showed that AaSho1 activates the MAPK pathway via AaSte11-AaPbs2-AaHog1. These results suggest that AaSho1 of *A. alternata* is essential for fungal development, pathogenesis and osmotic stress response by activating the MAPK cascade pathway via Sho1-Ste11-Pbs2-Hog1.

1. Introduction

The cuticle layer of plants is composed of waxes and cutin [1], which represent the outermost barrier that protects plants from desiccation, UV radiation, mechanical damage, pathogens and herbivores [2]. However, suitable cuticle chemistry is also a necessary factor for enabling host recognition and development of infection structures by phytopathogenic fungi [3]. In several phytopathogenic fungi, including *Magnaporthe grisea* and *Magnaporthe oryzae*, the cutin monomers and waxes are essential inducers of infection structure differentiation, particularly during appressorium formation stage [4,5]. Previous studies have shown that conidia of *Botrytis cinerea* have a higher germination rate on surfaces coated with apple wax and form appressoria more rapidly [6]. Tang et al. [7] found that 'Pingguoli' fruit waxes promote the appressorium differentiation and infection hyphae formation in *A. alternara*.

Meanwhile, in *Puccinia*, *Colletotrichum* and *Blumeria graminis*, conidial germination and appressorium formation were also induced by fruit waxes [8–10]. The stimulation of spore germination and appressorium formation in *B. graminis* by C_{24} and C_{25} alkane wax monomers was reported by Feng et al. [11]. Similarly, cutin monomers have an inductive effect on conidial germination and appressorium formation of *Ustilago maydis* [12]. Some studies have shown that the hydrophobicity of plant surfaces is also an essential physical signal for the induction of infection structure differentiation of phytopathogenic fungi [13]. For example, hard surface hydrophobicity are the unique physical signal for appressorium differentiation in *M. grisea* and *Colletotrichum gloeosporioides* [14]. Hydrophobicity can induce mycelial growth and appressorium differentiation in *U. maydis*, and hydrophobicity and other chemical signals are combined and co-induced more effectively [12]. However, the regulatory mechanisms by which phytopathogenic fungi recognize

and translate physical/chemical signals on the host surface to influence infection structure differentiation are not fully understood.

The MAPK signaling pathway is one of the most important and highly conserved signaling pathways found in eukaryotes [15], and its function is to be activated upon receipt of an extracellular signal stimulus and to transmit the signal into the nucleus to regulate the gene expression levels [15,16]. The high-osmolarity glycerol (HOG) MAPK pathway is specific for transducing environmental osmotic stress signals [17], and the Sho1 branch is one of the upstream branches of the HOG-MAPK pathway in *Saccharomyces cerevisiae* [18]. When transmembrane receptors are stimulated by extracellular signaling molecules, they initiate signaling cascades through upstream pathways and converge at the Pbs2 protein. Subsequently, Pbs2 protein phosphorylates Hog1-MAPK, leading to the activation of specific cellular responses, including intracellular glycerol synthesis and cell growth and development [19]. In *Fusarium graminearum*, FgSho1 activates the downstream Ste50-Ste11-Ste7 MAPK cascade signaling pathway to initiate the infection structural differentiation and mycotoxin production [20]. VdSho1 regulates growth and development, pathogenicity and oxidative stress response in *V. dahliae* by activating the downstream Vst50-Vst11-Vst7 MAPK cascade signaling pathway [21]. Interestingly, FgSho1 of *F. graminearum* is functionally distinct from its homologue in *S. cerevisiae*, recognising only cell wall integrity-related signals, but not in response to osmotic stress, and does not couple to the downstream HOG pathway for signaling [20]. Based on these results, we hypothesised that Sho1 may modulate virulence of phytopathogenic fungi through early signal recognition and activation of downstream signaling pathways, although the mode of recognition and regulation depends on the pathogen and the mutualistic system and has not been extensively studied in *A. alternata*.

Alternaria rot, caused by the fungus *Alternaria* sp. is a significant post-harvest issue that affects fruits, with incidence rates of up to 37 % during packing, transportation, and storage after harvesting [22]. Specifically, *A. alternata* is the primary pathogenic fungus responsible for *Alternaria* rot on pear fruit, and which is the main post-harvest disease affecting the 'Zaosu' pear (*Pyrus bretschneider* Rehd. cv. Zaosu) [22].

In this study, we used AaSho1, a transmembrane protein found in *A. alternata*, to systematically elucidate the molecular mechanisms underlying its recognition of wax and hydrophobic signals. We aimed to investigate AaSho1's role in regulating the differentiation of infection structures in *A. alternata*. These findings will provide valuable insights into understanding the molecular regulatory network by which this pathogen recognizes, responds to and transduces external signals, and initiates infection. They will also aid in the development of novel and environmentally friendly strategies for the effective control of *Alternaria* rot in pears.

2. Materials and methods

2.1. Fungal isolates and culture conditions

The WT strain of *A. alternata*, designated 'JT-03', was previously isolated from a diseased pear fruit grown at Tiaoshan farm (Jingtai Country, Gansu Province, China). The strains were grown at 28 ℃ on potato dextrose agar (PDA). Conidial suspensions were prepared by rinsing the 5 d old cultures with sterile water and were filtered through 4 layers of sterile cheesecloth to separate out mycelial fragments. Unless otherwise stated, the conidial concentrations were adjusted to 10^6 conidia mL^{-1} using a hemocytometer for experimental evaluations in *vitro* and in *vivo*.

2.2. Construction of mutant and complementation strains

AaSho1 deletion and complementation strains were generated using previously described protocols [23,24]. Identification of putative gene deletion mutants was performed by PCR (Fig. S1) and qRT-PCR (Fig. S2). Primers used to amplify gene fragments are listed in Table S1.

2.3. Vegetative growth, sporulation, biomass accumulation and pathogenicity assays

The conidial suspensions of ∆*AaSho1* and ∆*AaSho1-C* mutant strain were prepared and the conidial suspensions of WT was used as the control.

For vegetative growth measurements, the method of Yuan et al. [25] was used with minor modifications. Conidia of WT, ∆*AaSho1* and ∆*AaSho1-C* were inoculated onto the PDA plates and incubated at 28 ℃ for 3, 5 and 7 d. Colony diameters were measured by the 'cross' method and colony morphology was photographed. Each strain was replicated in quintuplicate.

For sporulation measurements, conidial suspensions of WT, ∆*AaSho1* and ∆*AaSho1-C* mutant strains incubated for 3 d on PDA medium were prepared by adding 15 mL of sterile water to each conidial suspension, diluted twice and counted under a microscope using a haemocytometer. For each treatment, three independent replicates were performed.

Conidial suspensions of WT, ∆*AaSho1* and ∆*AaSho1-C* mutant strains were inoculated onto PDA medium covered with sterile cellophane, and the cellophane was removed after 5 d incubation at 28 ℃ for biomass accumulation measurement. For each treatment, three independent replicates were performed.

Pathogenicity was determined by the method of Huang et al. [26].

2.4. Intracellular and extracellular melanin extraction and measurement

The method for crude melanin extraction was based on Wang et al. [27] with minor modifications. Strains were incubated in 100 mL of PDB medium at 28 ℃ for 6 d. Mycelia (for intracellular melanin) and filtrates (for extracellular melanin) were separated by using four layers of gauze. For each treatment, three independent replicates were performed.

2.5. Cell wall degrading enzymes (CWDEs) assay

Conidial suspensions of WT, ∆*AaSho1* and ∆*AaSho1-C* mutant were added to PDB medium and incubated for 4 d at 28 ℃ and 200 rpm. The hyphae were washed twice with sterile distilled water, then transferred to the medium containing pectin (Solarbio, #P8030) and Carboxymethyl cellulose sodium (Solarbio, #C8621) and further incubate in the dark for 0–9 d. CWDEs were measured using the assay kit (ploygalacturonase #BC2660, β-glucosidase #BC2560, cellulase #BC2540) (Solarbio Science & Technology, Beijing, China). For each treatment, three independent replicates were performed.

2.6. Stress response assay

Exogenous stress adaption was determined using the method of Ren et al. [28] with slight modifications. 1 M NaCl, 1 M sorbitol, 100 μM Congo red (CR), 0.01 % sodium dodecyl sulfate (SDS), 3 mM H_2O_2 and 2 mM menadione were added to the PDA. PDA without exogenous stress reagents was used as a control. 2 μL of WT, ∆*AaSho1* and ∆*AaSho1-C* mutant conidial suspensions were inoculated into the centre of PDA plates and incubated at 28 ℃ for 3, 5 and 7 d. Colony diameters were measured by the 'cross' method and colony morphology was photographed. Each strain was replicated in quintuplicate.

2.7. Intracellular glycerol content and mycotoxin production assays

WT, ∆*AaSho1* and complementary mutant strains were added to 100 mL of PDB and incubated for 48 h at 28 ℃ and 150 rpm. 0.8 M NaCl was added and incubated for 1 h. 0.1 g hyphae were harvested and ground in liquid nitrogen. Intracellular glycerol levels were measured using the Tissue Glycerol Content Assay Kit E1012 (Applygen Technologies Inc. Beijing, China) [28].

Mycotoxin extraction was performed according to Liu et al. [29] with minor modifications. WT, ∆*AaSho1* and ∆*AaSho1-C* strains were

cultured in PDA at 28 ℃ for 4 d, and ~0.5 g of hyphae were harvested and ground in liquid nitrogen. They were then homogenized with 2.5 mL of extraction buffer (acetonitrile: water: formic acid (4: 0.997: 0.003)). Mycotoxin determination was performed according to Huang et al. [26].

2.8. Conidial germination and appressorium formation assays

The pear fruit wax was extracted according to the method of Tang et al. [7]. Contact angle was measured as previously described [29]. Gelbond PAG films were obtained from Univ-bio (Shanghai, China). The cutin monomers 1, 16-hexadecanediol (Hex) and 16-hydroxyhexadecanoic acid (Hyd) were obtained from Sigma-Aldrich (Beijing, China). The conidial germination and appressorium formation rates was determined using the method of Huang et al. [26].

2.9. RNA-seq and qRT-PCR analyses

For RNA-seq analyses, total RNA isolated from conidial suspensions of WT, Δ*AaSho1* and Δ*AaSho1-C* mutant strains cultured on Gelbond PAG film coated with fruit wax for 6 h. The whole genome of *A. alternata* was download form NCBI (https://www.ncbi.nlm.nih.gov/datasets/taxonomy/5599/). The sequencing and transcriptome analyses were based on those of Li et al. [30] and Gai et al. [31]. For each treatment, three independent replicates were performed.

For qRT-PCR, the total RNA was collected through the TRIzol Universal Reagent (Accurate Biology, Hunan, China), and the First-strand cDNA was obtained by the Goldenstar™ RT6 cDNA Synthesis Mix

(Tsingke Biotechnology, Beijing, China). qRT-PCR was performed on the ABI7500 real-time thermal cycler (Applied Biosystems) using SYBR® Premix Ex TaqTM II (Tli RNaseH Plus) ROX plus (Takara, Dalian, China). The methods used to process the data are described in Qin et al. [32]. The qRT-PCR primers were listed in Table S1. For each treatment, three independent replicates were performed.

2.10. Yeast two-hybrid

Yeast two-hybrid system (YTH) analysis was performed as previously described [33]. Briefly, the full-length cDNAs of *AaCdc24*, *AaCdc42*, *AaSte11*, *AaSte50* and *AaPbs2* were cloned into the prey pGADT7 vector, and the full-length cDNAs of *AaSho1*, *AaPbs2* and *AaHog1* were cloned into the prey pGBKT7 vector (primers are shown in Table S2). The plasmid pairs were co-transformed into the yeast strain Y2H according to the Yeast Protocols Handbook (Clontech, USA). Two hybrid interaction-positive strains were verified by growth on QDO (SD-Leu/-Trp/-His/-Ade).

2.11. Data analysis

All statistical data were analysed using the 'Statsmodels' package (version 0.14.0) of Python 3.10.13. Graphs were plotted using the 'Matplotlib' (version 3.7.2) and 'Seaborn' (version 0.12.2) packages of Python 3.10.13. One-way analysis of variance and Tukey's honest significant difference test were used to assess statistically significant differences at the $p < 0.05$ level.
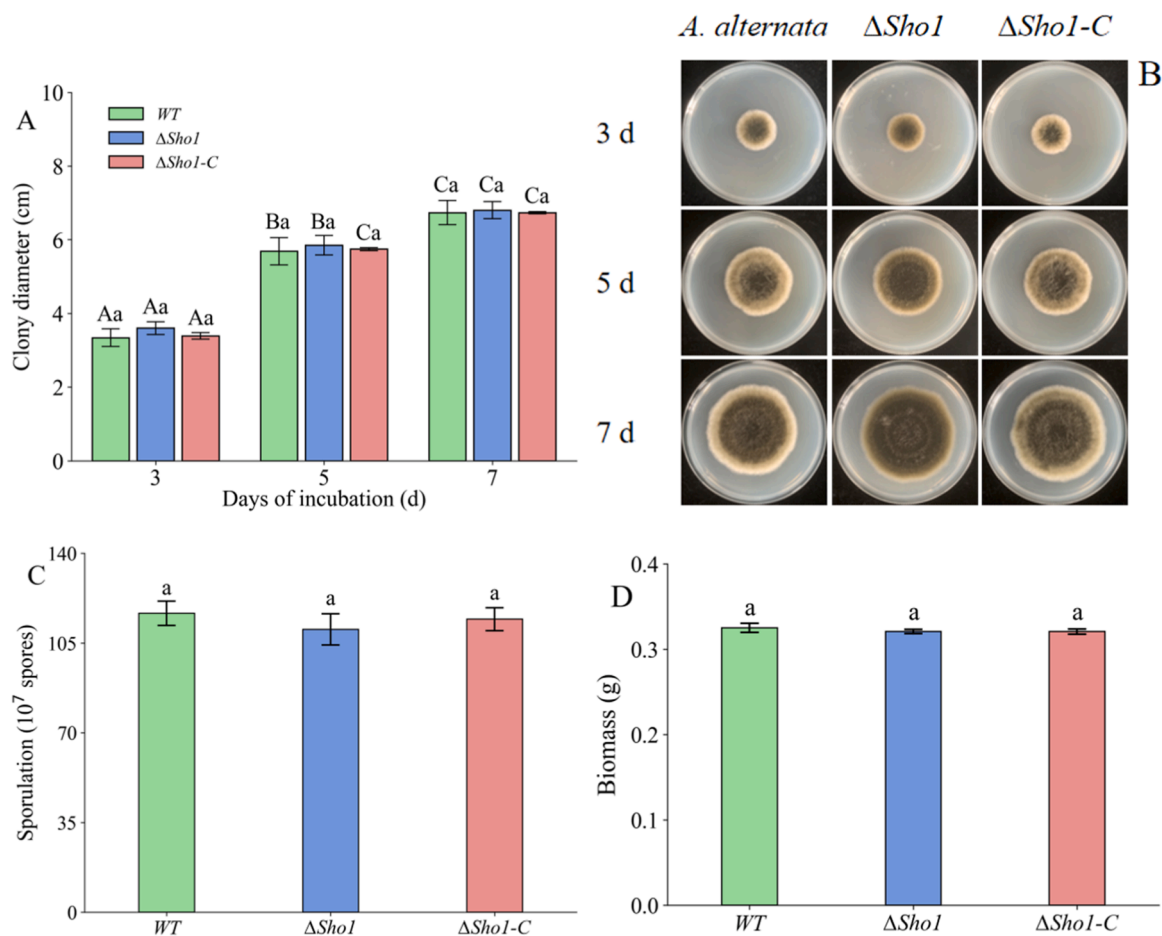
Fig. 1. Absence of Sho1 had no effect on *A. alternata* growth. Colony diameter (A), morphology (B), Spore production (C) and biomass (D) of WT, Δ*AaSho1* and Δ*AaSho1-C*. Vertical lines indicate standard error (± SD) of the means, and the uppercase letters indicate inter-group differences, lowercase letters indicate intra-group differences ($p < 0.05$).

3. Results

3.1. Aasho1 is essential for melanin production but dispensable for vegetative growth of A. alternata

As shown in Fig. 1A, the colony diameter increased with time for all strains, but there was no significant difference between the WT and Δ*AaSho1* mutant strain. The colony morphology of the Δ*AaSho1* mutant strain was deeper in colour compared to the WT (Fig. 1B), indicating that the *AaSho1* gene does not affect the growth of *A. alternata* colonies, but regulates colony morphology.

The conidial production of the Δ*AaSho1* mutant strain was slightly decreased but not significantly different from the WT (Fig. 1C). In addition, its biomass accumulation was also not significantly different from WT (Fig. 1D), indicating that the *AaSho1* gene is not involved in the regulating of conidial production and biomass accumulation of *A. alternata*.

The intracellular melanin content was significantly higher in the Δ*AaSho1* mutant strain compared to WT, which was 2.52 times higher than WT (Fig. 2A), indicating that the *AaSho1* gene plays a negative regulatory role in the synthesis of intracellular melanin. For the extracellular melanin content, the Δ*AaSho1* mutant strain showed a significant reduction of 51.77 % (Fig. 2C), suggesting that the *AaSho1* gene plays an important role in the extracellular secretion of melanin from *A. alternata*. The above results demonstrate that the *AaSho1* gene plays an important role in regulating the synthesis and secretion of melanin in *A. alternata*.

3.2. AaSho1 gene affects pathogenicity and CWDE activity of A. alternata

As shown in Fig. 3, the development *Alternaria* rot increased with the elongation of storage time, lesion diameter was lower in the Δ*AaSho1* mutant strain at 6 and 9 d compared to that of the WT, but the difference

was not significant. Nevertheless, it was observed that the lesion diameter of the Δ*AaSho1* mutant strain exhibited a notable reduction of 30.89 % compared to the WT strain after 12 d. These results suggest that the deletion of the *AaSho1* gene results in a delayed progression of the *Alternaria* rot. Furthermore, the restoration of the *AaSho1* gene in the complementary strain reversed this delay in disease development, confirming the functional role of *AaSho1* in this process.

Mainly CWDE activity of different strains were determined, the results showed that the β-GC, CL and PG enzyme activities of both WT and Δ*AaSho1* mutant strains tended to increase first and then decrease, and peaked at 6 d (Fig. 3). No significant difference in the β-GC activities was found between Δ*AaSho1* mutant strain and the WT (Fig. 3C). However, the CL activity of the Δ*AaSho1* mutant strain was reduced by 10.91 % ($p < 0.05$) compared to that of the WT at 9 d (Fig. 3D). Meanwhile, the PG activities of the Δ*AaSho1* mutant strain was reduced by 5.85 % and 11.38 % ($p < 0.05$) compared to WT at 6 and 9 d after incubation, respectively (Fig. 3E). These results suggest that both CL and PG activities are regulated by the AaSho1 in *A. alternata*.

3.3. The ΔAaSho1 mutant is hypersensitive to osmotic, oxidative stresses and cell wall-perturbing agents

Stress adaption of different strains were determined on PDA medium containing NaCl, sorbitol, CR, SDS, H_2O_2, and menadione, respectively (Fig. 4). In the presence of sorbitol, the colony diameters of the WT and Δ*AaSho1* mutant strains increased by 39.65 % and 34.77 % compared to those on PDA, respectively, and the colony diameter of the Δ*AaSho1* mutant strain decreased by 3.50 % compared to the WT ($p < 0.05$). In contrast, the colony diameter of the Δ*AaSho1* mutant strain was reduced by 16.17 %, 13.71 % and 7.03 % compared to WT in the presence of NaCl, CR and SDS, respectively ($p < 0.05$). In the presence of menadione, the WT growth was severely inhibited, whereas the Δ*AaSho1* mutant strain growth was totally inhibited. These results indicated that
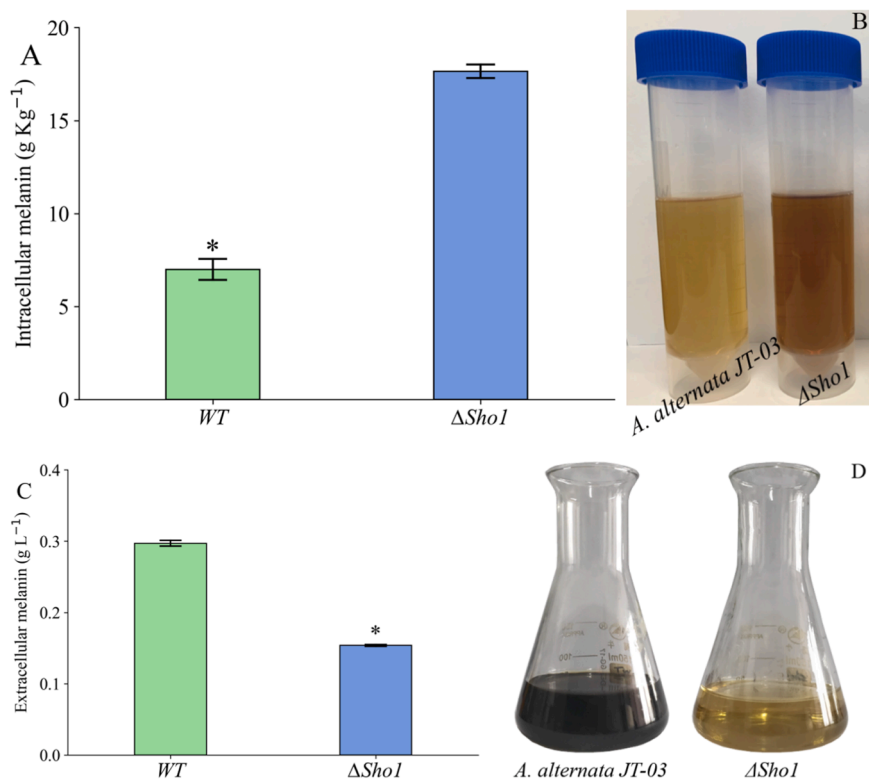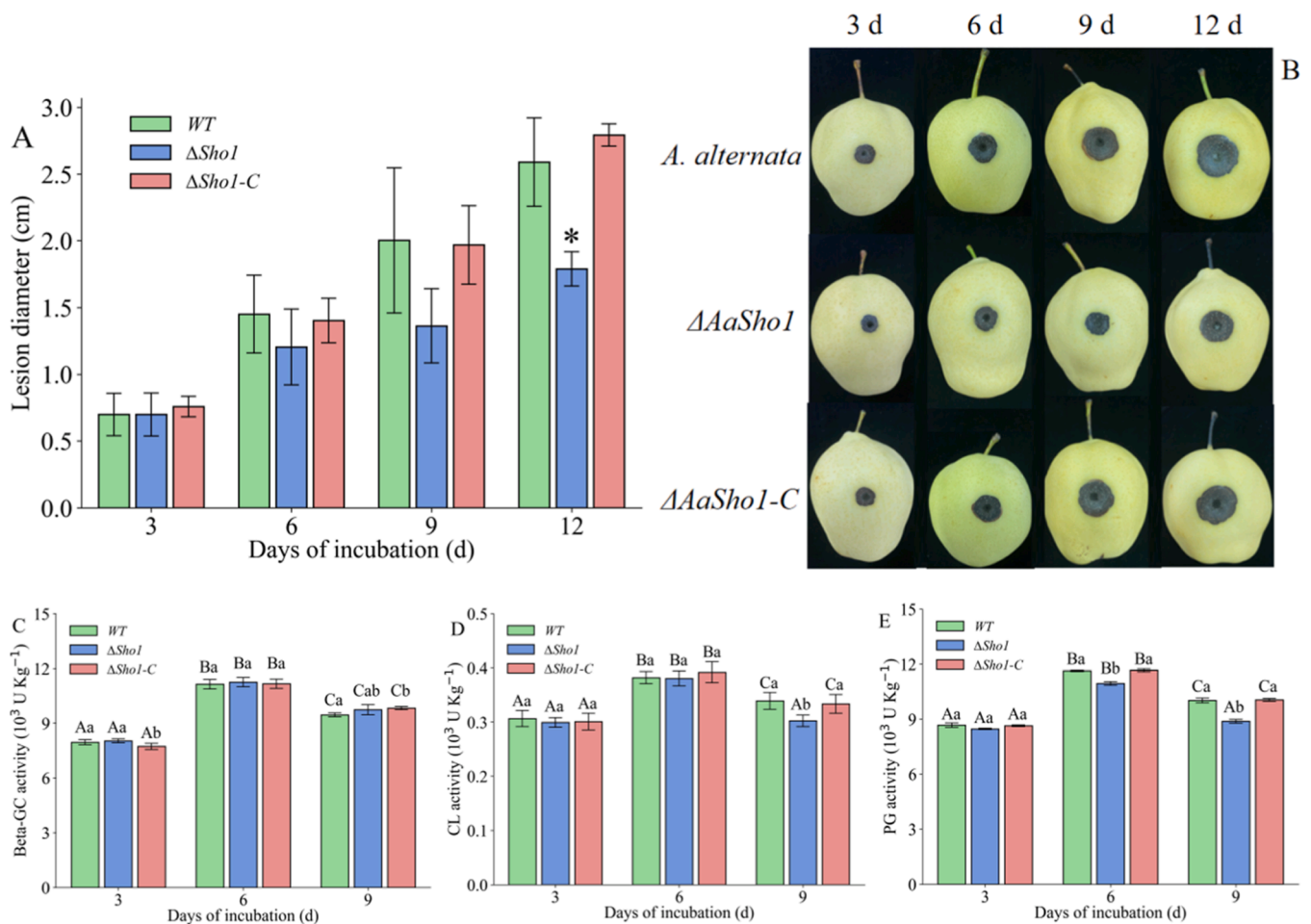

Fig. 2. Absence of Sho1 led to altered melanin production in *A. alternata*. Intracellular (A and B) and extracellular (C and D) melanin content of WT and Δ*AaSho1* mutant. Vertical lines indicate standard error ($\pm$ SD) of the means. Asterisks (*) denote a significant difference between the treatment and control at a level of $p < 0.05$.

Fig. 3. Sho1 deletion leads to changes in pathogenicity and enzyme activity of *A. alternata*. Disease diameter (A), black spot expansion (B), β-GC (C), CL (D) and PG (E) activity enzyme activities of WT, ΔAaSho1 and complementary mutant. Vertical lines indicate standard error (± SD) of the means. Asterisks (*) denote a significant difference between the treatment and control at a level of $p < 0.05$. The uppercase letters indicate inter-group differences, lowercase letters indicate intra-group differences ($p < 0.05$).

the AaSho1 participated in regulating the response to the exogenous stress regulation of formation by osmotic, oxidative stresses and cell wall-perturbing agents.

Intracellular glycerol content was further measured in the WT and ΔAaSho1 mutant strains in the presence of exogenous NaCl (Fig. 5). The intracellular glycerol content of the ΔAaSho1 mutant strain in PDB medium without NaCl was significantly lower than that of the WT. However, under NaCl stress, the intracellular glycerol content of the WT was up to 63.69 μmol g^{-1}, which was 4.3-fold higher than that in PDB, whereas that of the ΔAaSho1 mutant was merely 7.66 μmol g^{-1}. ΔAaSho1-C mutant strains restored this dicrease, this result further confirmed that AaSho1 was involved in osmotic stress adaption of *A. alternata*.

### 3.4. Mycotoxin production in A. alternata was differentially regulated by AaSho1

The mycotoxin content of the WT, ΔAaSho1 and ΔAaSho1-C mutant strains was determined by HPLC analysis. Tentoxin (TEN) toxin content in the ΔAaSho1 mutant strain significantly increased, which was 2.79 times higher than that of the WT (Fig. 6). But the ALT content was significantly reduced by 25.52 % compared to that of the WT. These results showed that the regulatory role of AaSho1 on mycotoxin production in *A. alternata* was dependent on the type of mycotoxin.

### 3.5. AaSho1 is involved infection structure differentiation of A. alternata

Hydrophilic surfaces were found to more effectively stimulate the conidial germination of the WT, ΔAaSho1, and ΔAaSho1-C mutant strains compared to hydrophobic surfaces. Notably, the difference in conidial germination rates between the WT and the ΔAaSho1 mutant strains on hydrophobic surfaces was not statistically significant, as illustrated in Fig. 7. The conidial germination rates of the WT, ΔAaSho1, and ΔAaSho1-C mutant strains exceeded 90 % after an 8 h incubation period. However, throughout the entire incubation period, the appressorium formation rate of the ΔAaSho1 mutant strain was significantly lower than that of the WT, as depicted in Fig. 7B. Specifically, the appressorium formation rate of the ΔAaSho1 mutant strain on the hydrophobic surface decreased by 50.51 % ($p < 0.05$) compared to the WT after an 8 h incubation period.

The fruit wax extract coated surface was more effective in inducing conidial germination and appressorium formation than that on the hydrophobicity surface with the same contact angle (Fig. 7). After 2 h incubation, conidial germination rates were up to 72.00 % and 70.00 % in the WT and ΔAaSho1 mutant strains, respectively, while the appressorium formation rate in the ΔAaSho1 mutant strain was reduced by 95.24 % compared to that of the WT ($p < 0.05$). The conidial germination rate of the WT and ΔAaSho1 mutant strains was over 92.00 % while the appressorium formation rate of the WT was 1.92 times higher ($p < 0.05$) than that of the ΔAaSho1 mutant strain after 8 h incubation.

In addition, in order to understand the stimulus role of fruit cutin
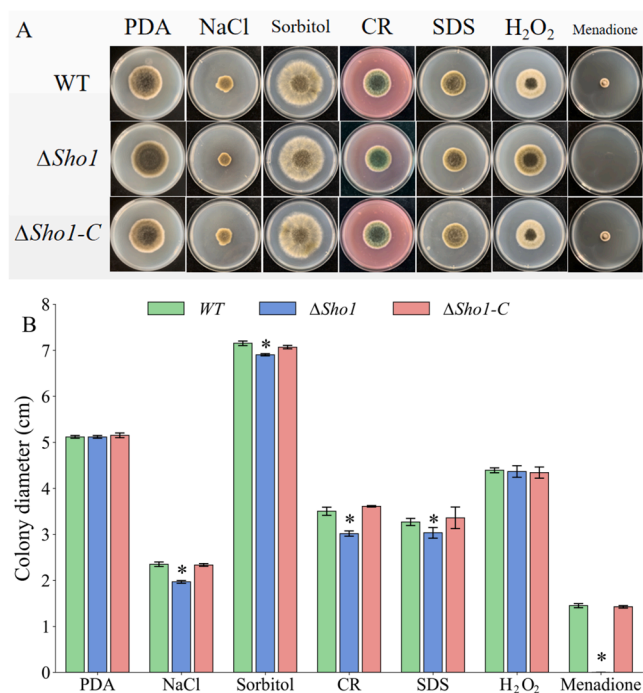
Fig. 4. Deletion of Sho1 causes changes in exogenous stress resistance in *A. alternata*. Colony morphology (A) and mycelial growth (B) of WT, Δ*AaSho1* and complementary mutant on PDA medium which supplemented with NaCl, Sorbitiol, CR, SDS, H₂O₂ and Menadione. Vertical lines indicate standard error (± SD) of the means, and the asterisks (*) denote a significant difference between the treatment and control at a level of $p < 0.05$.
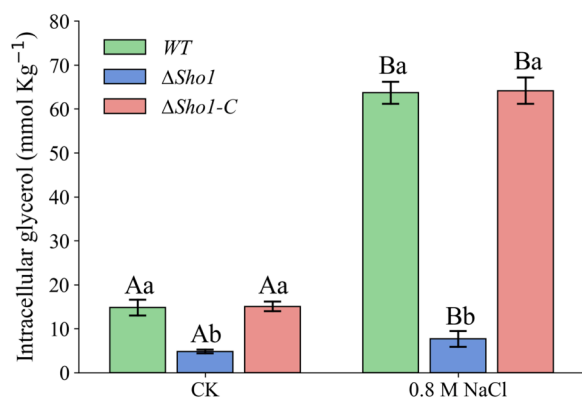
Fig. 5. Sho1 deletion produced changes in the intracellular glycerol content of WT, Δ*AaSho1* and complementary mutant. Vertical lines indicate standard error (± SD) of the means, and the uppercase letters indicate inter-group differences, lowercase letters indicate intra-group differences, different letters indicate significant differences ($p < 0.05$).

monomer on infection structure differentiation of *A. alternata*, conidial germination and appressorium formation rates were measured using Hex and Hyd, the results showed that the induction of cutin monomers was not as effective as that of fruit wax components (Fig. 8). Appressorium were barely formed at 2 h and the appressorium formation rate gradually increased with incubation time. As shown in Fig. 8B and D, the appressorium formation rate in the Δ*AaSho1* mutant strain was significantly lower than that in the WT throughout the incubation period. The appressorium formation rate of the WT on the Hex- and Hyd-coated surfaces was 2.9 and 3.4 times ($p < 0.05$) higher than that of the Δ*AaSho1* mutant, respectively, after 8 h incubation.

The infection structure formation of *A. alternata* was clearly observed
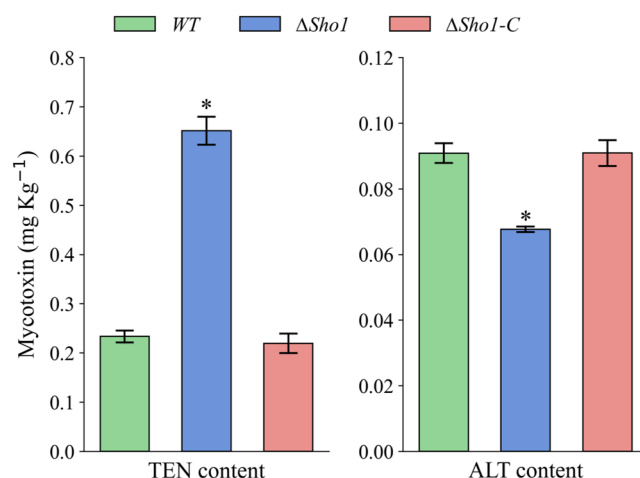
Fig. 6. Sho1 deletion produced changes in the mycotoxin content of WT, Δ*AaSho1* and complementary mutant. Vertical lines indicate standard error (± SD) of the means, and the asterisks (*) denote a significant difference between the treatment and control at a level of $p < 0.05$.

on the surface of the onion epidermis. As shown in Fig. 8, the fruit wax extract coated dewaxed onion epidermis had the strongest induction effect on conidial germination rate of the WT and Δ*AaSho1* mutant strain, followed by fruit wax extract coated onion epidermis, while the induction effect was less on the surface of onion epidermis and dewaxed onion epidermis alone, but there was no significant difference in the conidial germination rate of the Δ*AaSho1* mutant strain compared to the WT throughout the incubation period.

Appressoria were formed on the surface of fruit wax extract coated dewaxed onion epidermis and onion epidermis after 4 h incubation. The appressorium formation rates were 11.00 % and 6.33 % for the WT, respectively, whereas the Δ*AaSho1* mutant strain hardly formed appressoria at early stage ($p < 0.05$). After 8 h incubation, a large number of appressoria were formed on all four surfaces, but the inhibition of appressorium formation in the Δ*AaSho1* mutant was 25.00 %, 22.67 %, 31.25 % and 28.66 %, respectively ($p < 0.05$).

Infection hyphae formation of the WT and Δ*AaSho1* mutant strains on four onion epidermis surfaces was not observed during early stages (2–4 h incubation) (Fig. 8). The WT formed infection hyphae on the surface of onion epidermis, fruit wax extract coated onion epidermis and fruit wax extract coated dewaxed onion epidermis after 6 h incubation. However, at this time, the inhibition of infection hyphae formation rate of the Δ*AaSho1* mutant strain was 96.33 %, 94.74 % and 80.00 %, respectively. It was notable that the Δ*AaSho1* mutant strain exhibited a reduced infection hyphae formation rate compared to the WT up to 8 h incubation. Specifically, the infection hyphae formation rate of the Δ*AaSho1* mutant strain was 13.04 %, 35.38 %, 61.11 %, and 39.76 % of that observed in the WT, respectively.

3.6. AaSho1 regulates the expression of downstream Hog1-MAPK components

To understand the molecular mechanism by which AaSho1 regulates infection structure differentiation of *A. alternata* induced by fruit wax, transcriptome profiling of WT and Δ*AaSho1* mutant strains on fruit wax extract coated surface after 6 h incubation through RNA-seq. The total clean data obtained after filtering out low quality reads and adapter sequences was 38.81 GB. The total mapping ratio and uniquely mapping ratio were all above 75.00 % and 70.00 %, respectively (Table S3). These results indicate a high degree of sequencing accuracy. The conditions for screening DEGs were set as |FC= ≧ 2, FDR < 0.05 for WT and Sho1 samples. There were a total of 2764 DEGs, of which 1067 were up-regulated genes, accounting for 38.60 % of the total DEGs, and 1697
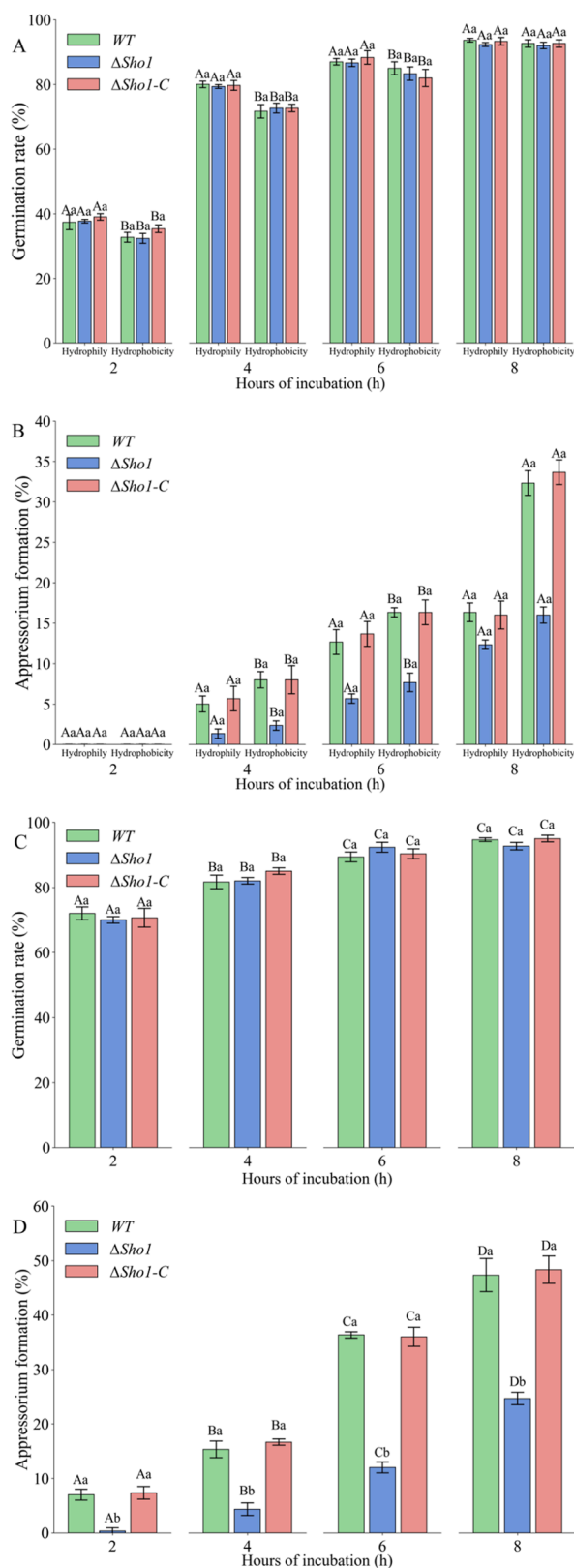
Fig. 7. Infection structure differentiation assays on hydrophobic or hydrophilic membranes and hydrophobic membrane with fruit wax. Spore germination rate and appressorium formation under hydrophily or hydrophobicity (A and B) and fruit wax (C and D) conditions of WT, Δ*AaSho1* and complementary mutant. Vertical lines indicate standard error (± SD) of the means, and the uppercase letters indicate inter-group differences, lowercase letters indicate intra-group differences, different letters indicate significant differences ($p < 0.05$).

were down-regulated genes, accounting for 61.40 % of the total DEGs, indicating that the DEGs showed predominant down-regulation (Fig. 9A). According to GO and KEGG annotation of DEGs [34,35], DEGs were found to be involved in different cascade pathways in *A. alternata* (Fig. 9B). The MAPK cascade pathway has 4 branches: pheromone, cell wall stress, high osmolarity and starvation (Fig. 9C). There were 53 DEGs, accounting for 1.92 % of the total number of DEGs, including 34 up-regulated genes and 19 down-regulated genes, accounting for 3.19 % and 1.12 % of the total number of up- and down-regulated DEGs, respectively. In the high osmolarity branch, the regulators *AaCdc24*, *AaCla4* and *AaSte11* downstream of the *AaSho1* gene were significantly up-regulated, whereas the regulator *AaSte50* was significantly down-regulated. It is speculated that the *AaSho1* gene may affect the Hog1-MAPK cascade pathway by regulating the expression of regulators in these pathway branches.

To verify the reliability of the RNA-Seq sequencing data, expression analysis of downstream regulators including *AaCdc24*, *AaCla4*, *AaSte50*, *AaSte11*, *AaPbs2* and *AaHog1* were assayed by qRT-PCR. The results showed that the gene expression levels of qRT-PCR were consistent with the results of RNA-Seq sequencing data (Fig. 9), demonstrating the authenticity and reliability of RNA-Seq sequencing data. As shown in Fig. 9, when the *AaSho1* gene was deleted, the expression levels of its downstream regulators *AaSte50* and *AaPbs2* were significantly decreased. In contrast, the expression levels of the regulators *AaCdc24*, *AaCla4* and *AaSte11* were significantly increased, and the expression level of *AaHog1* was reduced but not significantly. In particular, the expression level of *AaSte11* was increased when the *AaSho1* gene was deleted suggests that there are unknown genes that activate the *AaSte11* upon deletion of the *AaSho1*. These results indicated that the *AaSho1* gene could activate the AaPbs2-AaHog1-MAPK pathway, thereby initiating biological cellular functions in *A. alternata* that in turn affect appressorium formation, melanin and mycotoxin production, pathogenicity and resistance to exogenous stress.

3.7. AaSho1 activates the HOG-MAPK signaling pathway

The AaSho1 branch signaling pathway map of *A. alternata* was predicted based on the results of the RNA-seq analysis (Fig. S3). *AaSho1* first activates the *AaPbs2-AaHog1*-MAPK pathway by activating the downstream regulators *AaCdc42* and *AaSte20*, or by activating *AaSte50* to activate *AaSte11*, or directly after the fungus senses the external environmental signal stimulus.

The MAPK cascade pathway acts downstream of the transmembrane protein Sho1 sensor in phytopathogenic fungi, whereas Ste11 and Ste50 play an essential role in the entire MAPK cascade pathway as scaffolds [36]. To determine whether the AaSho1 protein signals to downstream proteins via AaSte11 and/or AaSte50, the YTH was used to characterise its interactions with downstream proteins. These results showed that AaSho1 showed physical interactions with AaSte50 and AaSte11, AaPbs2 with AaSte11 and AaHog1 with AaPbs2, while AaSho1 showed no physical interactions with AaCdc24, AaCdc42 and AaPbs2, while AaPbs2 showed no physical interactions with AaSte50 (Fig. 10A). In conclusion, *AaSho1* is an essential pathogenesis-related gene in *A. alternata* that positively regulates *AaSte50* and *AaSte11* to affect the *AaPbs2-AaHog1*-MAPK signaling pathway. Activation of the MAPK pathway in *A. alternata* resulted in the regulation of infection structure formation, melanin and mycotoxin content, CWDEs and resistance to exogenous stress, which in turn affects pathogenicity (Fig. 10B).

4. Discussion

Sho1, a signaling protein upstream of the HOG-MAPK signaling pathway, has a conserved structure [37]. This protein, homologous to *S. cerevisiae*, serves as a key regulator of the pathogenicity of phytopathogenic fungi. In *V. dahliae*, the *VdSho1*-mediated signaling pathway controls cotton plant colonisation and virulence by regulating
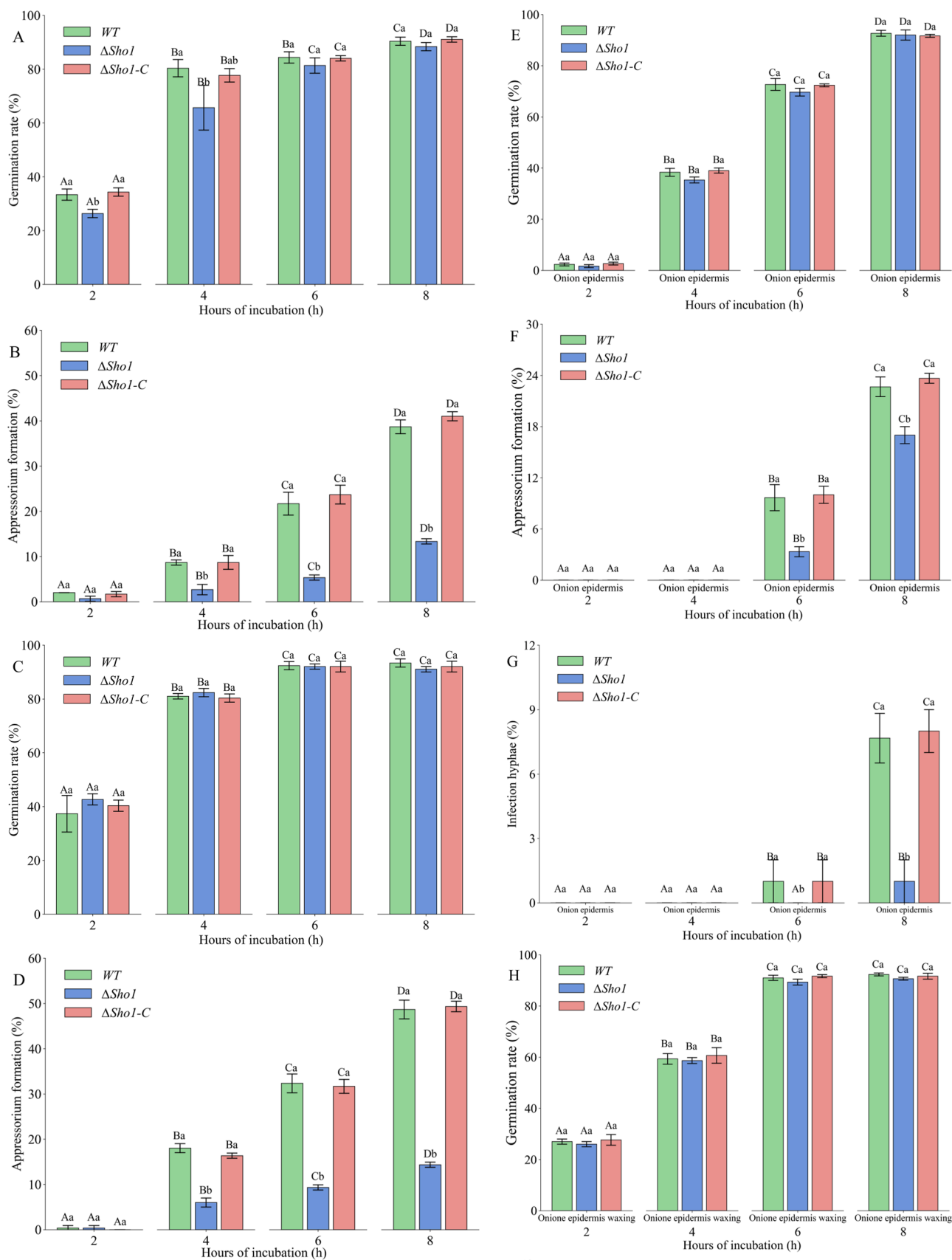
Fig. 8. Infection structure differentiation assays on hydrophobic membrane with 1, 16-hexadecanediol (A, B), 16-hydroxyhexadecanoic acid (C, D), onione epidermis (E, F, G), onione epidermis waxing (H, I, J), onione epidermis dewaxing (K, L, M) and dewaxed onione epidermis waxing (N, O, P). Vertical lines indicate standard error (± SD) of the means, and the uppercase letters indicate inter-group differences, lowercase letters indicate intra-group differences, different letters indicate significant differences ($p < 0.05$).
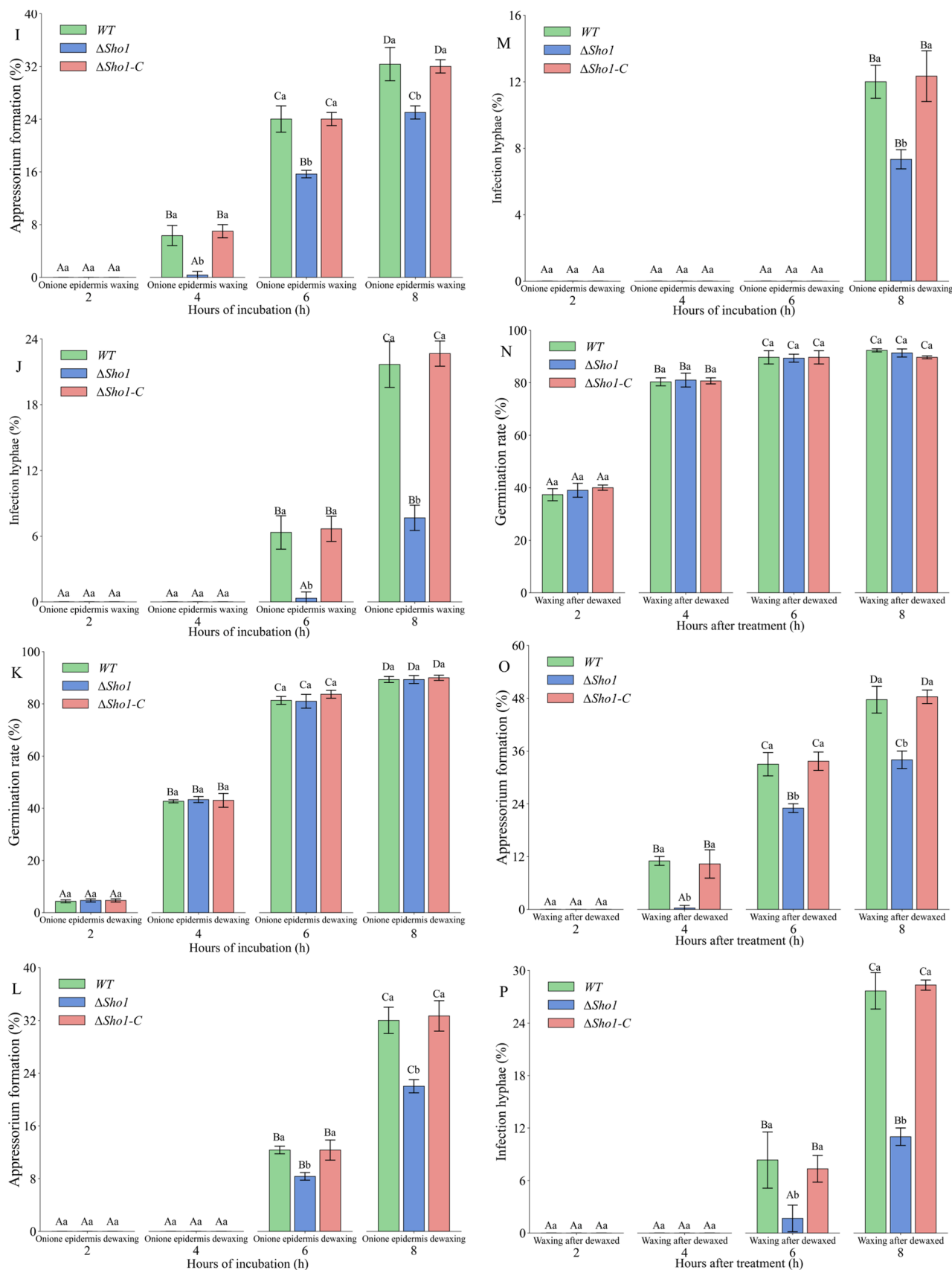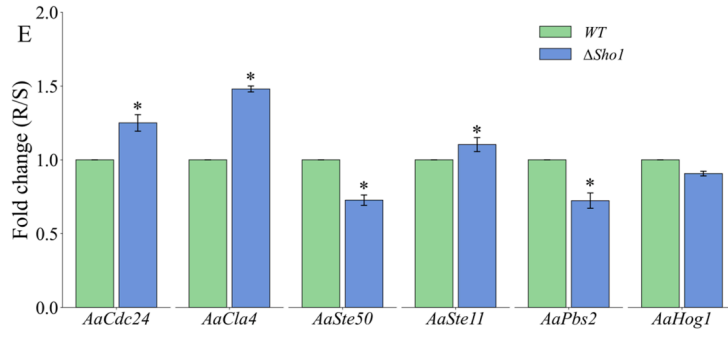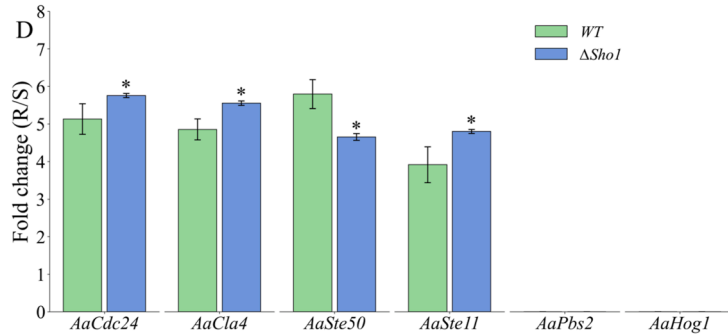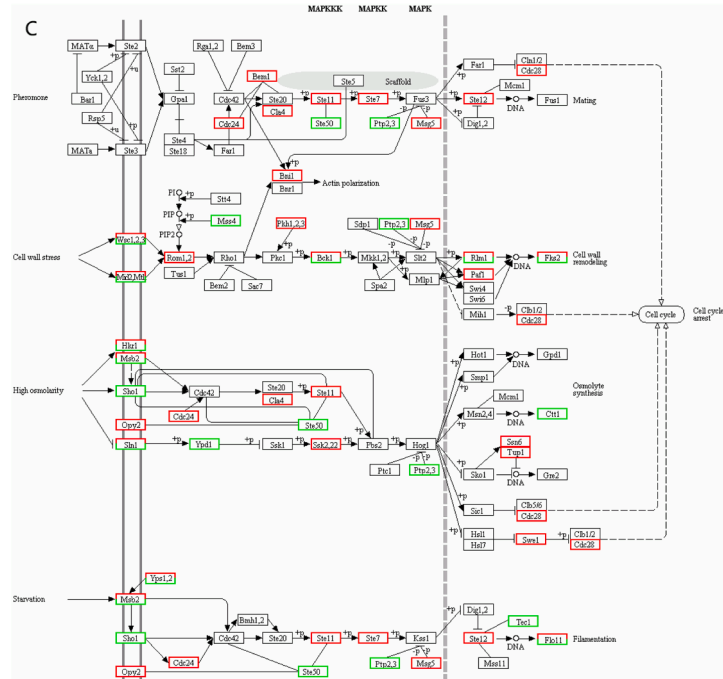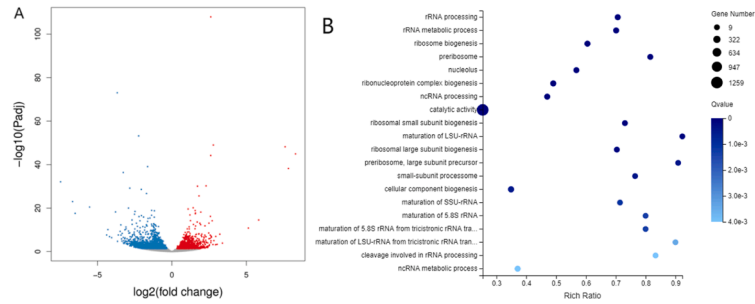
Fig. 8. (*continued*).

(caption on next page)

Fig. 9. Sho1 modulates the expression of MAPK pathway genes in *A. alternata*. A: differentially expressed gene volcano map of DEGs. B: GO enrichment analysis of DEGs. C: Schematic diagram of the MAPK cascade pathway regulated by AaSho1 gene. The red boxes indicate up-regulated genes, while the green boxes denote down-regulated genes in the ΔAaSho1 mutant compared to the WT. D and E: transcriptome-associated gene expression and expression levels of genes related to the downstream of AaSho1 gene by qRT-PCR. Vertical lines indicate standard error (± SD) of the means, and the asterisks (*) denote a significant difference between the treatment and control at a level of $p < 0.05$.
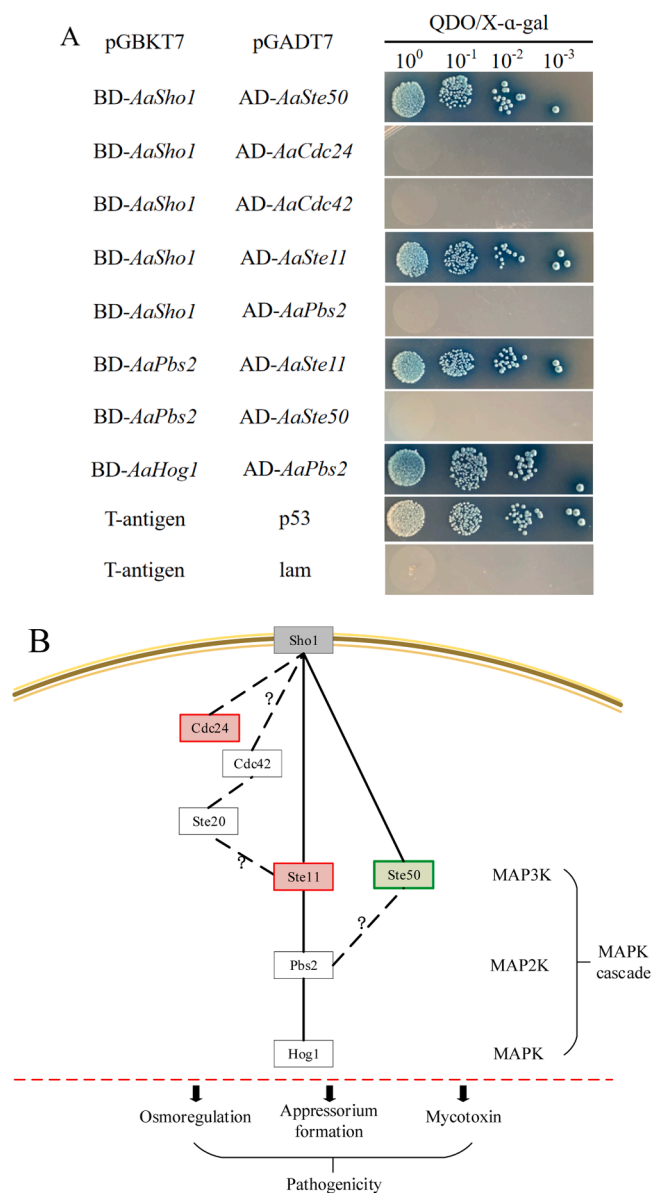
Fig. 10. Sho1 physically interacts with the protein of MAPK pathway. A: yeast two-hybrid identification of physical interactions between various genes. B: pattern of AaSho1 regulation of the *A. alternata* HOG-MAPK cascade pathway. The transmembrane protein AaSho1 can perceive external physicochemical signals, activating the *A. alternata* osmotic response, infection structure formation, and mycotoxin synthesis through the MAPK module Ste11-Pbs2-Hog1, thereby affecting the pathogenicity of *A. alternata*.

production, but showed significant differences in regulation of melanin synthesis and secretion, mycotoxin content, CWDEs, resistance to exogenous stress and pathogenicity. These results are not entirely consistent with the findings of previous studies, suggesting that AaSho1 in *A. alternata* still plays species-specific roles.

CWDE is one of the main pathogenic factors that phytopathogenic fungi use to invade and infect the host. Sensing signals from the host surface, the pathogenic fungus secretes CWDEs during mycelial growth and infection structural differentiation [39]. It has been found that the pathogenicity of *M. oryzae* is reduced when the gene encoding polygalacturonase is suppressed [40]. In *U. maydis*, membrane receptor proteins, upon sensing physical and/or chemical signals from the plant surface, induce the secretion of CWDEs to overcome the infection barriers posed by the plant cell wall [41]. In addition, the knockout mutant showed reduced CWDE activity during *A. alternata* infection of citrus, which also led to a reduction in its pathogenicity [42]. The present results showed that the CL and PG activities were significantly reduced compared to the WT, although the β-GC activity of the ΔAaSho1 mutant strain was not significantly different from that of the WT (Fig. 3C).

Mycotoxins, as secondary metabolites and a common virulence factor, are derived mainly from *Alternaria, Fusarium, Penicillium, Claviceps* and *Aspergillus* [43,44] and play an important role in host infection and colonisation [45]. Data presented in this study showed that the ΔAaSho1 mutant strain has a decrease in ALT toxin content and a slight increase in TEN toxin content (Fig. 6), which is consistent with the results of previous research. For instance, the regulation of mycotoxin synthesis in *F. graminearum* is attributed to the action of *FgSho1*, which activates the MAPK cascade signaling pathway [20]. Similarly, in *Aspergillus flavus*, mycotoxin production and pathogenicity are controlled by *AfSho1*, which activates the MAPK pathway via the downstream regulator *AfSte20* [46]. Additionally, the fungus utilises melanin, an important secondary metabolite, to regulate a variety of biological processes [47]. Beyond its role in fungal pathogenesis, melanin also confers protection against harsh environments and enhances stress resistance [48]. Compared to the WT, the ΔAaSho1 mutant strain had significantly lower extracellular melanin content, and however, its intracellular melanin content was significantly higher compared to that of WT. Taken together, these results confirm the involvement of *AaSho1* in the secondary metabolism of *A. alternata*. Meanwhile, the results of this study showed that the growth rate of the ΔAaSho1 mutant strain was not significantly different from the WT on PDA containing H_2O_2. However, it was significantly reduced on PDA containing NaCl, CR and SDS (Fig. 4). Simultaneously, the intracellular glycerol content of the ΔAaSho1 mutant strain was significantly reduced in both PDA with or without NaCl compared to that of the WT (Fig. 5). Therefore, based on the above results, we can speculate that AaSho1 may act as a receptor that affects melanin and toxin content, CWDE activities and regulates melanin secretion from intracellular to extracellular in response to certain external signals, ultimately affecting the pathogenicity of *A. alternata*.

The composition of the plant cuticle and its catabolic compounds influence fungal development and infection [49]. The multiple components of the cuticle have different effects on fungal infection. During plant-pathogen interactions, plant cuticle composition might be affected by pathogens which, conversely, can sense plant surface components and modulate their pathogenicity and virulence [6]. Many studies have shown that pathogen development (e.g. spore germination, germ tube elongation and appressorium formation) can be triggered by the recognition of the components of the wax [7]. For example, in

penetration and melanin biosynthesis [33]. In *B. cinerea*, the *BcSho1* branch plays a critical role in conidial production and virulence [28]. Interestingly, deletion of the *AaSho1* gene in the citrus pathogenic fungus *A. alternata* has shown little or no effect on osmotic and oxidative stress resistance, suggesting a limited role for the AaSho1 protein in this regard [38]. In the pear pathogenic *A. alternata* JT-03 presented in this study, the ΔAaSho1 mutant strain did not differ significantly in colony diameter and morphology, biomass accumulation and conidial

Colletotrichum gloeosporioides, the spore germination and appressorium formation can be triggered by the C24 primary alcohol on the surface of avocado fruit [50]. Longer primary alcohols such as 1-octacosanol (C28) and 1-triacontanol (C30) can induce appressorium formation of the rice blast fungus [51]. Sho1, as putative membrane sensor protein, is critical for external environmental stresses (osmotic, oxidative stresses) and plant surface signals (epicuticular waxes and cutin monomers, the physical nature of the surface, such as its hydrophobicity, hardness, and topography) recognition and activation of the MAPK in plant fungi [52]. During infection, membrane sensing proteins sense physical and/or chemical signals from the host surface and activate downstream signaling pathways to transduce signals from the extracellular environment to intracellular effector proteins, thereby differentiating the appressorium, which then penetrates the host epidermal cells and initiates infectious growth [53,54]. Of these, membrane sensing proteins are essential for the pathogenic fungus to recognise external stimuli and initiate infection. For example, the membrane sensing protein Pth11, upstream of the cAMP-PKA signaling pathway, is important for regulating appressorium formation in *M. grisea* [55]. In *Fusarium oxysporum*, deletion of the Ste2 receptor protein results in a partial loss of the ability to establish infective structures on the epidermal surface of plants [56]. The results of this study showed that the Δ*AaSho1* mutant strain significantly reduced appressorium formation rates on hydrophobic and wax-coated surfaces (Fig. 7). Meanwhile, the rates of appressorium formation and infection hyphae formation were also significantly lower in the Δ*AaSho1* mutant strain than in the WT on onion epidermis (Fig. 8). It is concluded that the reason for the reduced pathogenicity of the Δ*AaSho1* mutant strain is related to the defective development of infection structures. This is consistent with studies showing that *Sho1* in *M. oryzae* and *U. maydis* affects pathogenicity by regulating appressorium formation [56,57].

Phytopathogenic fungi have evolved well-developed physical/chemical signal sensing and transmission systems for the external environment and can adapt accordingly through recognition, transduction and response pathways [58]. The Hog-MAPK cascade pathway in *S. cerevisiae* initiated by the Sho1 signaling pathway typically requires the involvement of the Sho1 protein and its downstream regulators such as Ste11 and Ste50, which are ultimately transduced by Pbs2 (MAPKK) to Hog1 (MAPK) for convergence [59,60]. Previous studies have shown that the transmembrane protein Sho1 interacts with Ste11 to direct external environmental stress signals to the downstream Pbs2, which in turn activates the Hog-MAPK pathway to regulate and initiate cellular responses and increase intracellular glycerol levels to cope with the external high osmotic environment and improve adaptability [61,62]. In this study, through YTH experiments, the AaSho1 protein was shown to interact with AaSte50 and AaSte11 (Fig. 10). Meanwhile, physical interactions exist between AaSte11 and AaPbs2, and AaPbs2 and AaHog1, respectively. These results suggest that Sho1-Ste11-Pbs2-Hog1 is required for HOG-MAPK signaling pathway by the sensor protein AaSho1 in *A. alternata* (Fig. 10). This is consistent with previous research. For example, in *F. graminearum*, FgSho1 activates the MAPK cascade pathway via Ste50-Ste11-Ste7 as an intermediate regulator to regulate fungal development and pathogenicity [63]. In *Colletotrichum fructicola*, CfSte50 acts as an intermediate regulator of the MAPK cascade pathway and is required for growth, asexual reproduction, appressorium formation, pathogenicity and response to exogenous stress [64]. Meanwhile, Zarrinpar et al. [65] found that Ste11 can bind to a region at the C-terminus of Sho1, which in turn acts on Pbs2. However, in *S. cerevisiae*, O'Rourke et al. [66] modified the Sho1 pathway model to suggest that the Sho1 protein activates the MAPK cascade pathway by activating Ste20/Ste50 to activate Ste11-Pbs2-Hog1. Raitt et al. [67] found that the Sho1 protein moves Ste20 to the site of polarised growth via Cdc42, which activates the Pbs2-Hog1 MAPK pathway to complete the signaling process. In *Candida albicans*, the second branch of the Sho1 protein, parallel to Msb2, transduces the recognised signal to Cdc42-Ste20 (PAK)-Ste11 (MAPKKK)/Ste50, which in turn activates the

MAPK cascade pathway [68]. This is inconsistent with our findings, suggesting that the process of signaling by the Sho1 protein is species-specific.

In conclusion, phenotypic analysis of the Δ*AaSho1* mutant strain revealed that *AaSho1* has no significant effect on colony diameter and morphology, biomass accumulation or conidial yield of *A. alternata*. However, the mutant strain showed varying degrees of reduction in virulence, regulation of melanin synthesis and secretion, mycotoxin content, CWDEs and resistance to exogenous stress. Meanwhile, The Δ*AaSho1* mutant strain showed no significant changes in conidial germination rates on hydrophobic surfaces, pear fruit wax extract-, or cutin monomer-coated surfaces. Interestingly, the appressorium rate was significantly reduced, and in the onion epidermis simulation experiment, both the appressorium and infection hyphae formation rates of the Δ*AaSho1* mutant strain were significantly reduced. The yeast two-hybrid experiment demonstrated that the AaSho1 protein activates the MAPK cascade pathway through AaSte11-AaPbs2-AaHog1, thereby regulating the physiological functions of *A. alternata*, including infection structure differentiation, virulence, stress response, and secondary metabolite synthesis.

CRediT authorship contribution statement

Yang Bi: Software. **Dov B. Prusky:** Conceptualization. **Yongxiang Liu:** Writing – original draft, Writing – review & editing. **Jing Yuan:** Formal analysis. **Yongcai Li:** Funding acquisition, Project administration.

Declaration of Competing Interest

The authors declare that they have no known competing financial interests or personal relationships that could have appeared to influence the work reported in this paper, this work is an original research and the data presented in the manuscript has not been published elsewhere.

Acknowledgments

Appendix A. Supporting information

Supplementary data associated with this article can be found in the online version at doi:10.1016/j.csbj.2024.04.031.

References

[1] Spangenberg JE, Schweizer M, Zufferey V. Shifts in carbon and nitrogen stable isotope composition and epicuticular lipids in leaves reflect early water-stress in vineyards. Sci Total Environ 2020;739:140343. https://doi.org/10.1016/j.scitotenv.2020.140343.

[2] Domínguez E, Cuartero J, Heredia A. An overview on plant cuticle biomechanics. Plant Sci 2011;181:77–84. https://doi.org/10.1016/j.plantsci.2011.04.016.

[3] Skamnioti P, Gurr SJ. *Magnaporthe grisea* cutinase2 mediates appressorium differentiation and host penetration and is required for full virulence. Plant Cell 2007;19:2674–89. https://doi.org/10.1105/tpc.107.051219.

[4] Lee YH, Dean RA. cAMP regulates infection structure formation in the plant pathogenic fungus *Magnaporthe grisea*. Plant Cell 1993;5:693–700. https://doi.org/10.1105/tpc.5.6.693.

[5] Kong LA, Li GT, Liu Y, Liu MG, Zhang SJ, et al. Differences between appressoria formed by germ tubes and appressorium-like structures developed by hyphal tips in *Magnaporthe oryzae*. Fungal Genet Biol 2013;56:33–41. https://doi.org/10.1016/j.fgb.2013.03.006.

[6] Leroch M, Kleber A, Silva E, Coenen T, Koppenhöfer D, et al. Transcriptome profiling of *Botrytis cinerea* conidial germination reveals upregulation of infection-related genes during the prepenetration stage. Eukaryot Cell 2013;12:614–26. https://doi.org/10.1128/ec.00295-12.

[7] Tang Y, Li YC, Bi Y, Wang Y. Role of pear fruit cuticular wax and surface hydrophobicity in regulating the prepenetration phase of *Alternaria alternata* infection. J Phytopathol 2017;165:313–22. https://doi.org/10.1111/jph.12564.

[8] Atkinson TG, Allen PJ. Purification and partial characterization of a factor in cotton wax stimulating the germination of self-inhibited wheat stem rust uredospores. Plant Physiol 1966;41:28–33. https://doi.org/10.1104/pp.41.1.28.

[9] Podila GK, Rogers LM, Kolattukudy PE. Chemical signals from avocado surface wax trigger germination and appressorium formation in *Colletotrichum gloeosporioides*. Plant Physiol 1993;103:267–72. https://doi.org/10.1104/pp.103.1.267.

[10] Hansjakob A, Riederer M, Hildebrandt U. Wax matters: absence of very-long-chain aldehydes from the leaf cuticular wax of the glossy11 mutant of maize compromises the prepenetration processes of *Blumeria graminis*. Plant Pathol 2011; 60:1151–61. https://doi.org/10.1111/j.1365-3059.2011.02447.x.

[11] Feng J, Wang F, Liu GS, Greenshields D, Shen WY, et al. Analysis of a *Blumeria graminis*-secreted lipase reveals the importance of host epicuticular wax components for fungal adhesion and development. Mol Plant-Microbe Inter 2009; 22:1601–10. https://doi.org/10.1094/MPMI-22-12-1601.

[12] Mendoza A, Berndt P, Djamei A, Weise C, Linne U, et al. Physical-chemical plant-derived signals induce differentiation in *Ustilago maydis*. Mol Microbiol 2009;71: 895–911. https://doi.org/10.1111/j.1365-2958.2008.06567.x.

[13] Liu H, Suresh A, Willard FS, Siderovski DP, Lu S, et al. Rgs1 regulates multiple Gα subunits in *Magnaporthe* pathogenesis, asexual growth and thigmotropism. EMBO J 2007;26:690–700. https://doi.org/10.1038/sj.emboj.7601536.

[14] Talbot NJ. On the trail of a cereal killer: exploring the biology of *Magnaporthe grisea*. Annu Rev Microbiol 2003;57:177–202. https://doi.org/10.1146/annurev. micro.57.030502.090957.

[15] Rispail N, Soanes DM, Ant C, Czajkowski R, Grünler A, et al. Comparative genomics of MAP kinase and calcium-calcineurin signalling components in plant and human pathogenic fungi. Fungal Genet Biol 2009;46:287–98. https://doi.org/10.1016/j. fgb.2009.01.002.

[16] Ma DM, Li RY. Current Understanding of HOG-MAPK Pathway in *Aspergillus fumigatus*. Mycopathologia 2012;175:13–23. https://doi.org/10.1007/s11046-012-9600-5.

[17] Hohmann S. Control of high osmolarity signalling in the yeast *Saccharomyces cerevisiae*. FEBS Lett 2009;583:4025–9. https://doi.org/10.1016/j. febslet.2009.10.069.

[18] Yang YY, Xie PD, Li YC, Bi Y, Prusky DB. Updating insights into the regulatory mechanisms of calcineurin-activated transcription factor Crz1 in pathogenic fungi. J Fungi 2022;8:1082. https://doi.org/10.3390/jof8101082.

[19] Yaakov G, Duch A, García-Rubio M, Clotet J, Jimenez J, et al. The stress-activated protein kinase Hog1 mediates S phase delay in response to osmostress. Mol Biol Cell 2009;20:3572–82. https://doi.org/10.1091/mbc.e09-02-0129.

[20] Gu Q, Chen Y, Liu Y, Zhang CQ, Ma ZH. The transmembrane protein FgSho1 regulates fungal development and pathogenicity via the MAPK module Ste50-Ste11-Ste7 in *Fusarium graminearum*. N Phytol 2015;206:315–28. https://doi.org/10.1111/nph.13158.

[21] Qi XY, Zhou S, Shang XG, Wang XY. *VdSho1* regulates growth, oxidant adaptation and virulence in *Verticillium dahliae*. J Phytopathol 2016;164:1064–74. https://doi.org/10.1111/jph.12527.

[22] Li YC, Bi Y, An LZ. Occurrence and latent infection of *Alternaria* Rot of Pingguoli pear (*Pyrus bretschneideri* Rehd. cv. Pingguoli) fruits in Gansu, China. J Phytopathol 2006;155:56–60. https://doi.org/10.1111/j.1439-0434.2006.01202.x.

[23] Ren WC, Zhang ZH, Shao WY, Yang YL, Zhou MG, et al. The autophagy-related gene *BcATG1* is involved in fungal development and pathogenesis in *Botrytis cinerea*. Mol Plant Pathol 2017;18:238–48. https://doi.org/10.1111/mpp.12396.

[24] Ma HJ, Li L, Gai YP, Zhang XY, Chen YN, et al. Histone acetyltransferases and deacetylases are required for virulence, conidiation, DNA damage repair, and multiple stresses resistance of *Alternaria alternata*. Front Microbiol 2021;12: 783633. https://doi.org/10.3389/fmicb.2021.783633.

[25] Yuan J, Chen Z, Guo ZQ, Li D, Zhang F, et al. PbsB regulates morphogenesis, aflatoxin B1 biosynthesis, and pathogenicity of *Aspergillus flavus*. Front Cell Infect Microbiol 2018;8:162. https://doi.org/10.3389/fcimb.2018.00162.

[26] Huang Y, Li YC, Li DM, Bi Y, Prusky DB, et al. Phospholipase C from *Alternaria alternata* is induced by physiochemical cues on the pear fruit surface that dictate infection structure differentiation and pathogenicity. Front Microbiol 2020;11: 1279. https://doi.org/10.3389/fmicb.2020.01279.

[27] Wang F, Gao WD, Sun JY, Mao XW, Liu KX, et al. NADPH oxidase ClNOX2 regulates melanin-mediated development and virulence in *Curvularia lunata*. Mol Plant-Microbe Inter 2020;11:1315–29. https://doi.org/10.1094/MPMI-06-20-0138-R.

[28] Ren WC, Liu N, Yang YL, Yang QQ, Chen CJ, et al. The sensor proteins BcSho1 and BcSln1 are involved in, though not essential to, vegetative differentiation, pathogenicity and osmotic stress tolerance in *Botrytis cinerea*. Front Microbiol 2019;10:328. https://doi.org/10.3389/fmicb.2019.00328.

[29] Liu YX, Li YC, Ma L, Deng HW, Huang Y, et al. The transmembrane protein AaSho1 is essential for appressorium formation and secondary metabolism but dispensable for vegetative growth in pear fungal *Alternaria alternata*. Fungal Biol 2022;126: 139–48. https://doi.org/10.1016/j.funbio.2021.11.006.

[30] Li S, Tian YH, Wu K, Ye YF, Yu JP, et al. Modulating plant growth-metabolism coordination for sustainable agriculture. Nature 2018;560:595–600. https://doi. org/10.1038/s41586-018-0415-5.

[31] Gai YP, Li L, Ma HJ, Riely BK, Liu B, et al. Critical role of MetR/MetB/MetC/MetX in cysteine and methionine metabolism, fungal development, and virulence of *Alternaria alternata*. e01911-20 Appl Environ Microbiol 2021;87. https://doi.org/10.1128/AEM.01911-20.

[32] Qin L, Li D, Zhao JR, Yang G, Wang YC, et al. The membrane mucin Msb2 regulates aflatoxin biosynthesis and pathogenicity in fungus *Aspergillus flavus*. Micro Biotechnol 2020;14:628–42. https://doi.org/10.1111/1751-7915.13701.

[33] Li JJ, Zhou L, Yin CM, Zhang DD, Klosterman SJ, et al. The *Verticillium dahliae* Sho1-MAPK pathway regulates melanin biosynthesis and is required for cotton infection. Environ Microbiol 2019;21:4852–74. https://doi.org/10.1111/1462-2920.14846.

[34] Ashburner M, Ball CA, Blake JA, Botstein D, Butler H, et al. Gene ontology: tool for the unification of biology. Nat Genet 2000;25:25–9. https://doi.org/10.1038/75556.

[35] Altermann E, Klaenhammer TR. PathwayVoyager: pathway mapping using the Kyoto Encyclopedia of Genes and Genomes (KEGG) database. BMC Genom 2005;6: 60. https://doi.org/10.1186/1471-2164-6-60.

[36] Seet BT, Pawson T. MAPK signaling: sho business. Curr Biol 2004;14:R708–10. https://doi.org/10.1016/j.cub.2004.08.044.

[37] De Nadal E, Posas F. The HOG pathway and the regulation of osmoadaptive responses in yeast. FEMS Yeast Res 2022;22:1–7. https://doi.org/10.1093/femsyr/foac013.

[38] Yu PL, Chen LH, Chung KR. How the pathogenic fungus *Alternaria alternata* copes with stress via the response regulators SSK1 and SHO1. e0149153 Plos One 2016; 11. https://doi.org/10.1371/journal.pone.0149153.

[39] Kubicek CP, Starr TL, Glass NL. Plant cell wall-degrading enzymes and their secretion in plant-pathogenic fungi. Annu Rev Phytopathol 2014;52:427–51. https://doi.org/10.1146/annurev-phyto-102313-045831.

[40] Quoc NB, Bao Chau NN. The role of cell wall degrading enzymes in pathogenesis of *Magnaporthe oryzae*. Curr Protein Pept Sci 2017;18:1019–34. https://doi.org/10.2174/1389203717666160813164955.

[41] Lanver D, Berndt P, Tollot M, Naik V, Vranes M, et al. Plant surface cues prime *Ustilago maydis* for biotrophic development. PLOS Pathog 2014;10:e1004272. https://doi.org/10.1371/journal.ppat.1004272.

[42] Chung KR. Mitogen-activated protein kinase signaling pathways of the tangerine pathotype of *Alternaria alternata*. MAP Kinase 2013;2:e4. https://doi.org/10.4081/mk.2013.e4.

[43] Eskola M, Altieri A, Galobart J. Overview of the activities of the European Food Safety Authority on mycotoxins in food and feed. World Mycotoxin J 2018;11: 277–89. https://doi.org/10.3920/WMJ2017.2270.

[44] Assunção R, Viegas S. Mycotoxin exposure and related diseases. Toxins 2020;12: 172. https://doi.org/10.3390/toxins12030172.

[45] Kang Y, Feng HW, Zhang JX, Chen SG, Valverde BE, et al. TeA is a key virulence factor for *Alternaria alternata* (Fr.) Keissler infection of its host. Plant Physiol Biochem 2017;115:73–82. https://doi.org/10.1016/j.plaphy.2017.03.002.

[46] Li D, Qin L, Wang YC, Xie QC, Li N, et al. AflSte20 regulates morphogenesis, stress response, and aflatoxin biosynthesis of *Aspergillus flavus*. Toxins 2019;11:730. https://doi.org/10.3390/toxins11120730.

[47] Aranda C, Méndez I, Barra PJ, Hernández-Montiel L, Fallard A, et al. Melanin induction restores the pathogenicity of *Gaeumannomyces graminis* var. *tritici* in wheat plants. J Fungi 2023;9:350. https://doi.org/10.3390/jof9030350.

[48] Liversage J, Coetzee MPA, Bluhm BH, Berger DK, Crampton BG. LOVe across kingdoms: blue light perception vital for growth and development in plant-fungal interactions. Fungal Biol Rev 2017;32:86–103. https://doi.org/10.1016/j. fbr.2017.11.003.

[49] Hansjakob A, Riederer M, Hildebrandt U. Appressorium morphogenesis and cell cycle progression are linked in the grass powdery mildew fungus *Blumeria graminis*. Fungal Biol 2012;116:890–901. https://doi.org/10.1016/j.funbio.2012.05.006.

[50] Arya GC, Sarkar S, Manasherova E, Aharoni A, Cohen H. The plant cuticle: an ancient guardian barrier set against long-standing rivals. Front Plant Sci 2021;12: 663165. https://doi.org/10.3389/fpls.2021.663165.

[51] Sadat MA, Han JH, Kim S, Lee YH, Kim KS, et al. The membrane-bound protein, MoAfo1, is involved in sensing diverse signals from different surfaces in the rice blast fungus. Plant Pathol J 2021;37:87–98. https://doi.org/10.5423/PPJ. OA.08.2020.0154.

[52] Román E, Nombela C, Pla J. The Sho1 adaptor protein links oxidative stress to morphogenesis and cell wall biosynthesis in the fungal pathogen *Candida albicans*. Mol Cell Biol 2005;25:10611–27. https://doi.org/10.1128/MCB.25.23.10611-10627.2005.

[53] Dohlman HG. Thematic minireview series: complexities of cellular signaling revealed by simple model organisms. J Biol Chem 2016;291:7786–7. https://doi. org/10.1074/jbc.R116.722934.

[54] Hagiwara D, Sakamoto K, Abe K, Gomi K. Signaling pathways for stress responses and adaptation in *Aspergillus* species: stress biology in the post-genomic era. Biosci Biotechnol Biochem 2016;80:1667–80. https://doi.org/10.1080/09168451.2016.1162085.

[55] Qian B, Su XT, Ye ZY, Liu XY, Liu MX, et al. MoErv14 mediates the intracellular transport of cell membrane receptors to govern the appressorial formation and pathogenicity of *Magnaporthe oryzae*. PLOS Pathog 2023;19:e1011251. https://doi.org/10.1371/journal.ppat.1011251.

[56] Liu WD, Zhou XY, Li GT, Li L, Kong LG, et al. Multiple plant surface signals are sensed by different mechanisms in the rice blast fungus for appressorium formation. PLoS Pathog 2011;7:e1001261. https://doi.org/10.1371/journal. ppat.1001261.

[57] Lanver D, Mendoza-Mendoza A, Brachmann A, Kahmann R. Sho1 and Msb2-related proteins regulate appressorium development in the smut fungus *Ustilago maydis*. Plant Cell 2010;22:2085–101. https://doi.org/10.1105/tpc.109.073734.

[58] Bahn YS, Xue CY, Idnurm A, Rutherford JC, Heitman J, et al. Sensing the environment: lessons from fungi. Nat Rev Microbiol 2007;5:57–69. https://doi.org/10.1038/nrmicro1578.

[59] Saito H, Tatebayashi K. Regulation of the osmoregulatory HOG MAPK cascade in yeast. J Food Biochem 2004;136:267–72. https://doi.org/10.1093/jb/mvh135.

[60] Tatebayashi K, Yamamoto K, Tanaka K, Tomida T, Maruoka T, et al. Adaptor functions of Cdc42, Ste50, and Sho1 in the yeast osmoregulatory HOG MAPK pathway. EMBO J 2006;25:3033–44. https://doi.org/10.1038/sj.emboj.7601192.

[61] Zarrinpar A, Park SH, Lim WA. Optimization of specificity in a cellular protein interaction network by negative selection. Nature 2003;426:676–80. https://doi.org/10.1038/nature02178.

[62] Zhu XG, Guo J, He FX, Zhang Y, Tan CL, et al. Silencing PsKPP4, a MAP kinase kinase kinase gene, reduces pathogenicity of the stripe rust fungus. Mol Plant Pathol 2018;19:2590–602. https://doi.org/10.1111/mpp.12731.

[63] Zheng DW, Zhang SJ, Zhou XY, Wang CF, Xiang P, et al. The *FgHOG1* pathway regulates hyphal growth, stress responses, and plant infection in *Fusarium graminearum*. PloS One 2012;7:e49495. https://doi.org/10.1371/journal.pone.0049495.

[64] Chen YY, Liu JA, Jiang SQ, Li H, Zhou GY. *Colletotrichum fructicola* STE50 is required for vegetative growth, asexual reproduction, appressorium formation,

pathogenicity and the response to external stress. J Plant Pathol 2020;102:335–42. https://doi.org/10.1007/s42161-019-00422-3.

[65] Zarrinpar A, Bhattacharyya RP, Nittler MP, Lim WA. Sho1 and Pbs2 act as coscaffolds linking components in the yeast high osmolarity MAP kinase pathway. Mol Cell 2004;14:825–32. https://doi.org/10.1016/j.molcel.2004.06.011.

[66] O'Rourke SM, Herskowitz I, O'Shea EK. Yeast go the whole HOG for the hyperosmotic response. Trends Genet 2002;18:405–12. https://doi.org/10.1016/S0168-9525(02)02723-3.

[67] Raitt DC, Posas F, Saito H. Yeast Cdc42 GTPase and Ste20 PAK-like kinase regulate Sho1-dependent activation of the Hog1 MAPK pathway. EMBO J 2000;19:4623–31. https://doi.org/10.1093/emboj/19.17.4623.

[68] Román E, Cottier F, Ernst JF, Pla J. Msb2 signaling mucin controls activation of Cek1 mitogen-activated protein kinase in *Candida albicans*. Eukaryot Cell 2009;8:1235–49. https://doi.org/10.1128/EC.00081-09.